Nano-Hexapod on the micro-station

Dehaeze Thomas

November 13, 2024

Contents

Now that the nano-hexapod is mounted and that a good multi-body model of the nano-hexapod The system is validated on the ID31 beamline.

At the beginning of the project, it was planned to develop a long stroke 5-DoF metrology system to measure the pose of the sample with respect to the granite. The development of such system was complex, and was not completed at the time of the experimental tests on ID31. To still validate the developed nano active platform and the associated instrumentation and control architecture, a 5-DoF short stroke metrology system was developed (Section 1).

The identify dynamics of the nano-hexapod fixed on top of the micro-station was identified for different experimental conditions (payload masses, rotational velocities) and compared with the model (Section 2).

Decentralized Integral Force Feedback is then applied to actively damp the plant in a robust way (Section **??**).

High authority control is then applied

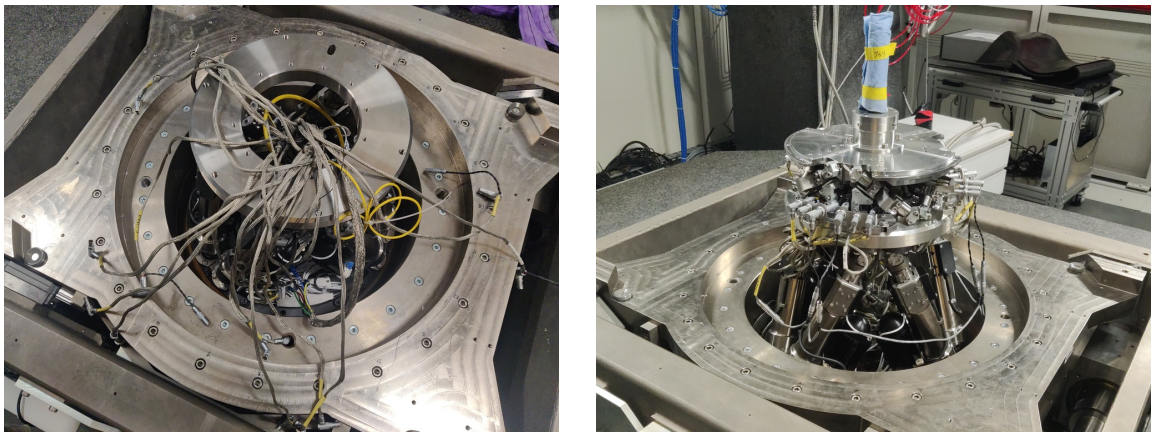

(a) Micro-station and nano-hexapod cables **(b)** Nano-hexapod fixed on top of the micro-station

Figure 1: Picture of the micro-station without the nano-hexapod (a) and with the nano-hexapod (b)

1 Short Stroke Metrology System

The control of the nano-hexapod requires an external metrology system measuring the relative position of the nano-hexapod top platform with respect to the granite. As the long-stroke ($\approx 1\,cm^3$) metrology system was not developed yet, a stroke stroke ($> 100\,\mu m^3$) was used instead to validate the nano-hexapod control.

A first considered option was to use the "Spindle error analyzer" shown in Figure 1.1a. This system comprises 5 capacitive sensors which are facing two reference spheres. As the gap between the capacitive sensors and the spheres is very small[1], the risk of damaging the spheres and the capacitive sensors is high.

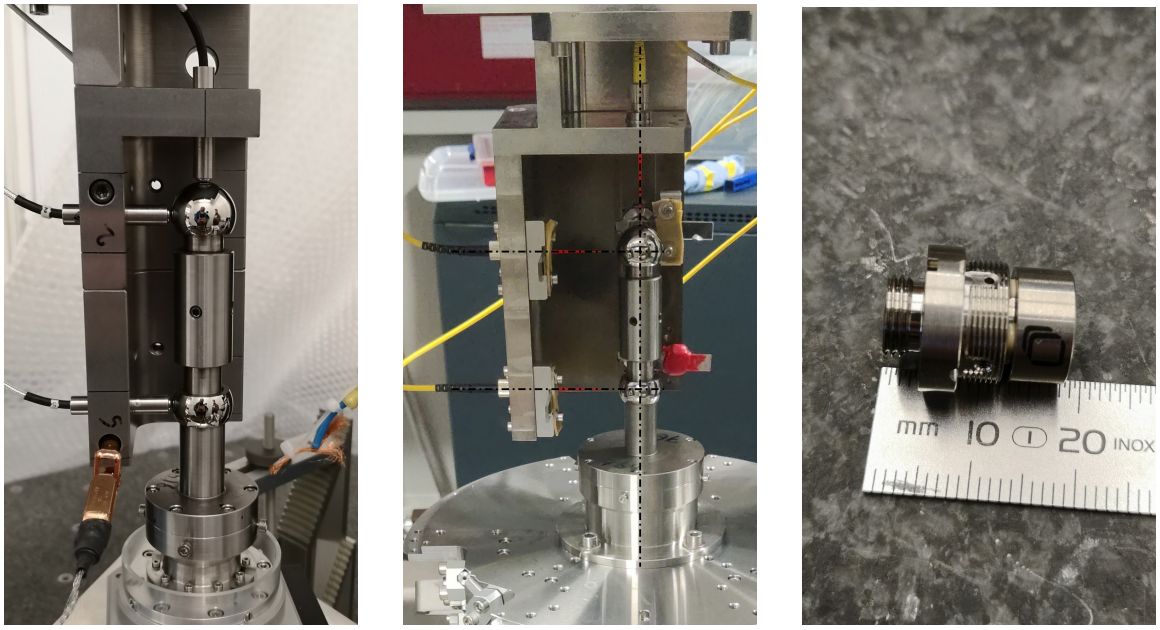

(a) Capacitive Sensors **(b)** Short-Stroke metrology **(c)** Interferometer head

Figure 1.1: Short stroke metrology system used to measure the sample position with respect to the granite in 5DoF. The system is based on a "Spindle error analyzer" (a), but the capacitive sensors are replaced with fibered interferometers (b). Interferometer heads are shown in (c)

Instead of using capacitive sensors, 5 fibered interferometers were used in a similar way (Figure 1.1b). At the end of each fiber, a sensor head[2] (Figure 1.1c) is used, which consists of a lens precisely positioned with respect to the fiber's end. The lens is focusing the light on the surface of the sphere, such that it

[1] Depending on the measuring range, gap can range from $\approx 1\,\mu m$ to $\approx 100\,\mu m$
[2] M12/F40 model from Attocube

comes back to the fiber and produces an interference. This way, the gap between the sensor and the reference sphere is much larger (here around $40\,mm$), removing the risk of collision.

Nevertheless, the metrology system still has limited measurement range, as when the spheres are moving perpendicularly to the beam axis, the reflected light does not coincide with the incident light, and for some perpendicular displacement, the interference is too small to be detected.

1.1 Metrology Kinematics

The developed short-stroke metrology system is schematically shown in Figure 1.2. The point of interest is indicated by the blue frame $\{B\}$, which is located $H = 150\,mm$ above the nano-hexapod's top platform. The spheres have a diameter $d = 25.4\,mm$, and indicated dimensions are $l_1 = 60\,mm$ and $l_2 = 16.2\,mm$. In order to compute the pose of the $\{B\}$ frame with respect to the granite (i.e. with respect to the fixed interferometer heads), the measured small displacements $[d_1,\ d_2,\ d_3,\ d_4,\ d_5]$ by the interferometers are first written as a function of the small linear and angular motion of the $\{B\}$ frame $[D_x,\ D_y,\ D_z,\ R_x,\ R_y]$ (1.1).

$$d_1 = D_y - l_2 R_x, \quad d_2 = D_y + l_1 R_x, \quad d_3 = -D_x - l_2 R_y, \quad d_4 = -D_x + l_1 R_y, \quad d_5 = -D_z \tag{1.1}$$

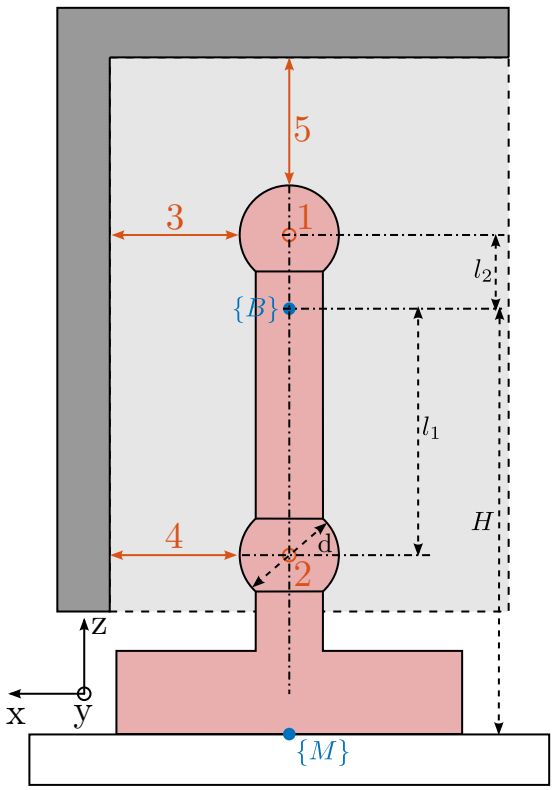

Figure 1.2: Schematic of the measurement system. Measured distances are indicated by red arrows.

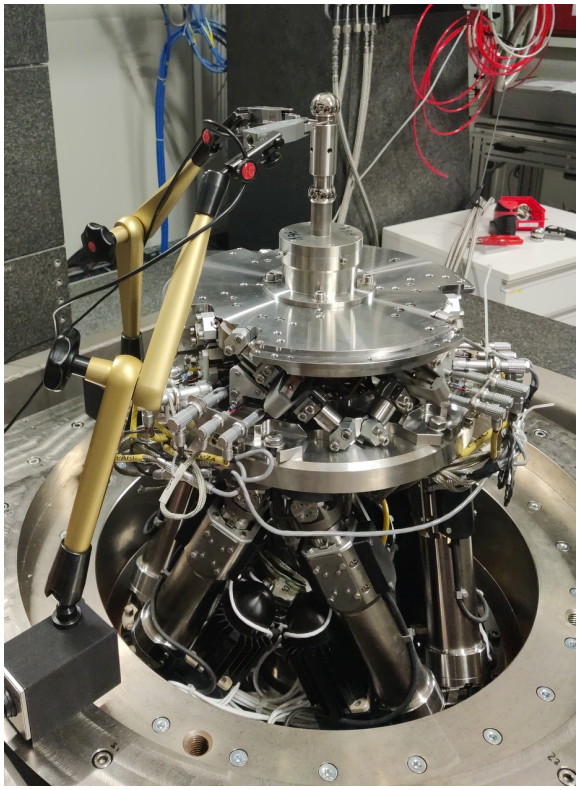

Figure 1.3: The top sphere is aligned with the rotation axis of the spindle using two probes.

The five equations (1.1) can be written in a matrix form, and then inverted to have the pose of $\{B\}$ frame as a linear combination of the measured five distances by the interferometers (1.2).

$$\begin{bmatrix} D_x \\ D_y \\ D_z \\ R_x \\ R_y \end{bmatrix} = \begin{bmatrix} 0 & 1 & 0 & -l_2 & 0 \\ 0 & 1 & 0 & l_1 & 0 \\ -1 & 0 & 0 & 0 & -l_2 \\ -1 & 0 & 0 & 0 & l_1 \\ 0 & 0 & -1 & 0 & 0 \end{bmatrix}^{-1} \cdot \begin{bmatrix} d_1 \\ d_2 \\ d_3 \\ d_4 \\ d_5 \end{bmatrix} \tag{1.2}$$

1.2 Rough alignment of the reference spheres

The two reference spheres are aligned with the rotation axis of the spindle. To do so, two measuring probes are used as shown in Figure 1.3.

To not damage the sensitive sphere surface, the probes are instead positioned on the cylinder on which the sphere is mounted. First, the probes are fixed to the bottom (fixed) cylinder to align its axis with the spindle axis. Then, the probes are fixed to the top (adjustable) cylinder, and the same alignment is performed.

With this setup, the precision of the alignment of both sphere better with the spindle axis is expected to limited to $\approx 10\,\mu m$. This is probably limited due to the poor coaxiality between the cylinders and the spheres. However, the alignment precision should be enough to stay in the acceptance of the interferometers.

1.3 Tip-Tilt adjustment of the interferometers

The short stroke metrology system is placed on top of the main granite using a gantry made of granite blocs to have good vibration and thermal stability (Figure 1.4).

The interferometers need to be aligned with respect to the two reference spheres to approach as much as possible the ideal case shown in Figure 1.2. The vertical position of the spheres is adjusted using the micro-hexapod to match the height of the interferometers. Then, the horizontal position of the gantry is adjusted such that the coupling efficiency (i.e. the intensity of the light reflected back in the fiber) of the top interferometer is maximized. This is equivalent as to optimize the perpendicularity between the interferometer beam and the sphere surface (i.e. the concentricity between the beam and the sphere center).

The lateral sensor heads (i.e. all except the top one), which are each fixed to a custom tip-tilt adjustment mechanism, are individually oriented such that the coupling efficient is maximized.

1.4 Fine Alignment of reference spheres using interferometers

Thanks to the good alignment of the two reference spheres with the spindle axis and to the fine adjustment of the interferometers orientations, the interferometer measurement is made possible during

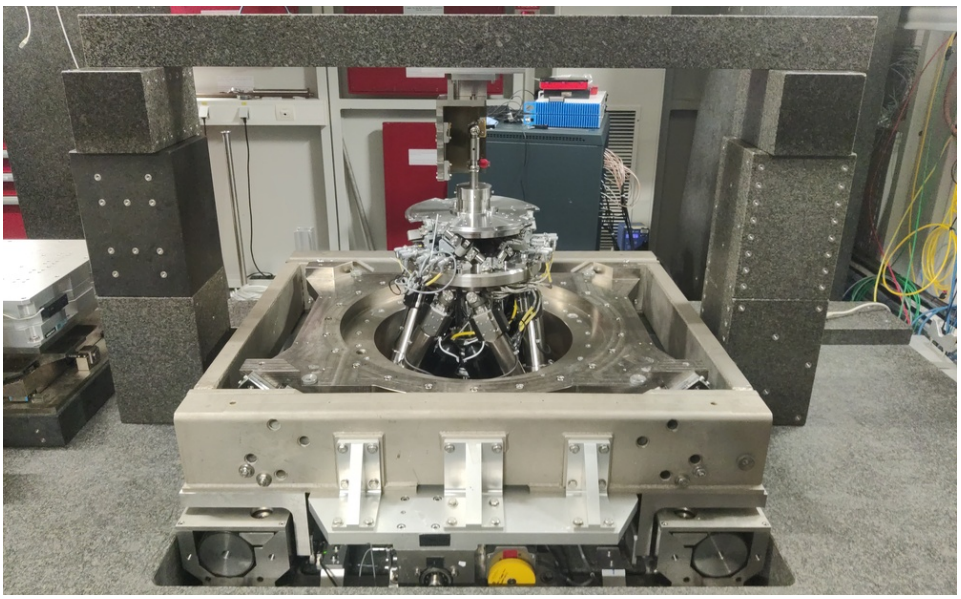

Figure 1.4: Granite gantry used to fix the short-stroke metrology system

complete spindle rotation. This metrology and therefore be used to better align the axis defined by the two spheres' center with the spindle axis.

The alignment process is made by few iterations. First, the spindle is scanned and the alignment errors are recorded. From the errors, the motion of the micro-hexapod to better align the spheres is determined and the micro-hexapod is moved. Then, the spindle is scanned again, and the new alignment errors are recorded.

This iterative process is first perform for angular errors (Figure 1.5a) and then for lateral errors (Figure 1.5b). Remaining error after alignment is in the order of $\pm 5\,\mu$rad for angular errors, $\pm 1\,\mu m$ laterally and less than $0.1\,\mu m$ vertically.

1.5 Estimated measurement volume

Because the interferometers are pointing to spheres and not flat surfaces, the lateral acceptance is limited. In order to estimate the metrology acceptance, the micro-hexapod is used to perform three accurate scans of $\pm 1\,mm$, respectively along the the x, y and z axes. During these scans, the 5 interferometers are recorded, and the ranges in which each interferometer has enough coupling efficiency for measurement are estimated. Results are summarized in Table 1.1. The obtained lateral acceptance for pure displacements in any direction is estimated to be around $+/-0.5\,mm$, which is enough for the current application as it is well above the micro-station errors to be actively corrected.

1.6 Estimated measurement errors

When using the NASS, the accuracy of the sample's positioning is linked to the accuracy of the external metrology. However, to validate the nano-hexapod with the associated instrumentation and control

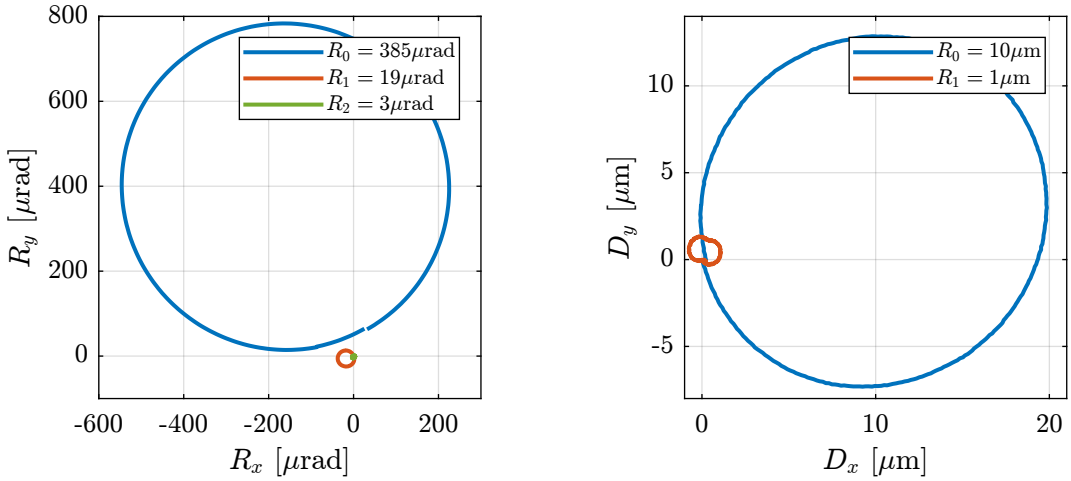

(a) Angular alignment

(b) Lateral alignment

Figure 1.5: Measured angular (a) and lateral (b) errors during a full spindle rotation. Between two rotations, the micro-hexapod is adjusted to better align the two spheres with the rotation axis.

Table 1.1: Estimated measurement range for each interferometer, and for three different directions.

	D_x	D_y	D_z
d_1 (y)	$1.0\,mm$	$> 2\,mm$	$1.35\,mm$
d_2 (y)	$0.8\,mm$	$> 2\,mm$	$1.01\,mm$
d_3 (x)	$> 2\,mm$	$1.06\,mm$	$1.38\,mm$
d_4 (x)	$> 2\,mm$	$0.99\,mm$	$0.94\,mm$
d_5 (z)	$1.33\,mm$	$1.06\,mm$	$> 2\,mm$

architecture, the accuracy of the metrology is not an issue. Only the bandwidth and noise characteristics of the external metrology are important. Yet, some elements effecting the accuracy of the metrology are discussed here.

First, the "metrology kinematics" (discussed in Section 1.1) is only approximate (i.e. valid for very small displacements). This can be seen when performing lateral $[D_x,\, D_y]$ scans using the micro-hexapod while recording the vertical interferometer (Figure 1.6a). As the interferometer is pointing to a sphere and not to a plane, lateral motion of the sphere is seen as a vertical motion by the top interferometer.

Then, the reference spheres have some deviations with respect to an ideal sphere. They are meant to be used with capacitive sensors which are integrating the shape errors over large surfaces. When using interferometers, the size of the "light spot" on the sphere surface is a circle with a diameter $\approx 50\,\mu m$, therefore the system is more sensitive to shape errors with small features.

As the interferometer light is travelling in air, the measured distance is sensitive to any variation in the refractive index of the air. Therefore, any variation of air temperature, pressure or humidity will induce measurement errors. For a measurement length of $40\,mm$, a temperature variation of $0.1\,^oC$ induces an errors in the distance measurement of $\approx 4\,nm$.

Finally, even in vacuum and in the absence of target motion, the interferometers are affected by noise [1]. The effect of the noise on the translation and rotation measurements is estimated in Figure 1.6b.

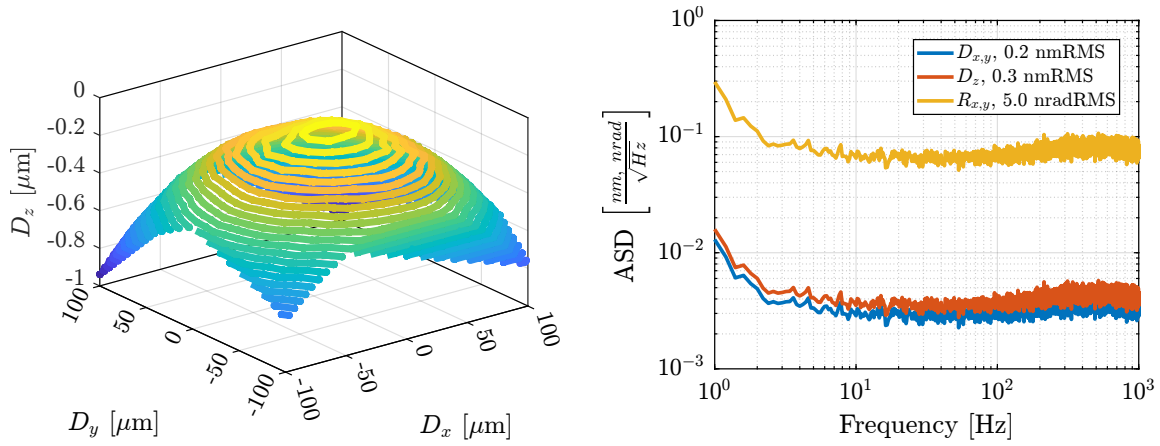

(a) Z measurement during an XY mapping

(b) Interferometer noise

Figure 1.6: Estimated measurement errors of the metrology. Cross-coupling between lateral motion and vertical measurement is shown in (a). Effect of interferometer noise on the measured translations and rotations is shown in (b).

2 Identified Open Loop Plant

2.1 First Open-Loop Plant Identification

The plant dynamics is first identified for a fixed spindle angle (at 0 deg) and without any payload. The model dynamics is also identified in the same conditions.

A first comparison between the model and the measured dynamics is done in Figure 2.1. A good match can be observed for the diagonal dynamics (except the high frequency modes which are not modeled). However, the coupling for the transfer function from command signals $\mathbf{u}$ to estimated strut motion from the external metrology $e\mathcal{L}$ is larger than expected (Figure 2.1a).

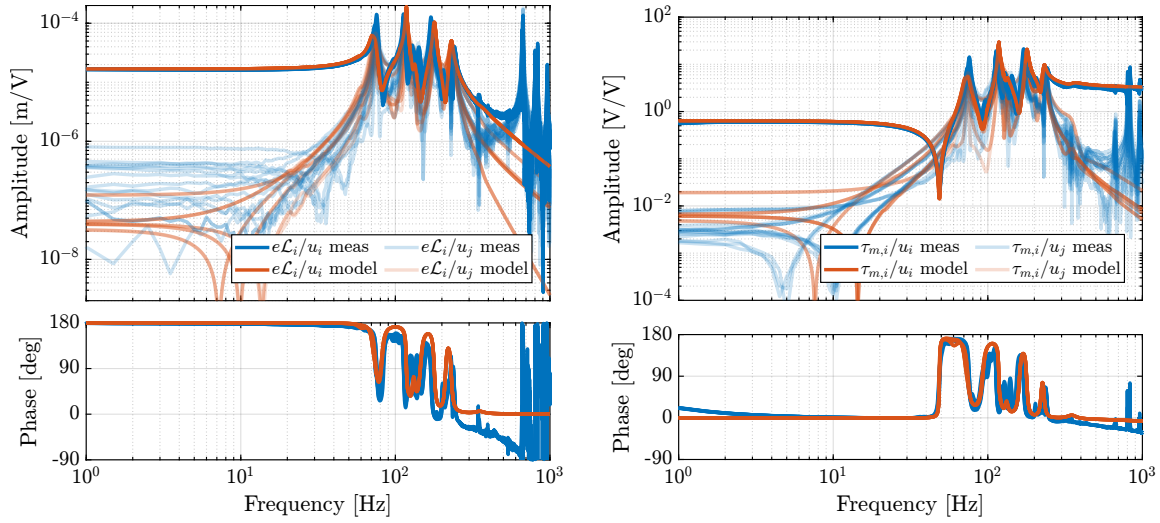

(a) External Metrology

(b) Force Sensors

Figure 2.1: Comparison between the measured dynamics and the multi-body model dynamics. Both for the external metrology (a) and force sensors (b).

2.2 Better Angular Alignment

One possible explanation of the increased coupling observed in Figure 2.1a is the poor alignment between the external metrology axes (i.e. the interferometer supports) and the nano-hexapod axes. To estimate this alignment, a decentralized low-bandwidth feedback controller based on the nano-hexapod encoders is implemented. This allowed to perform two straight movements of the nano-hexapod along the x and y axes in the frame of the nano-hexapod. During these two movements, the external metrology measurement is recorded and shown in Figure 2.2. It was found that there is a misalignment of 2.7

degrees (rotation along the vertical axis) between the interferometer axes and nano-hexapod axes. This was corrected by adding an offset to the spindle angle. To check that the alignment has improved, the same movement was performed using the nano-hexapod while recording the signal of the external metrology. Results shown in Figure 2.2b are indeed indicating much better alignment.

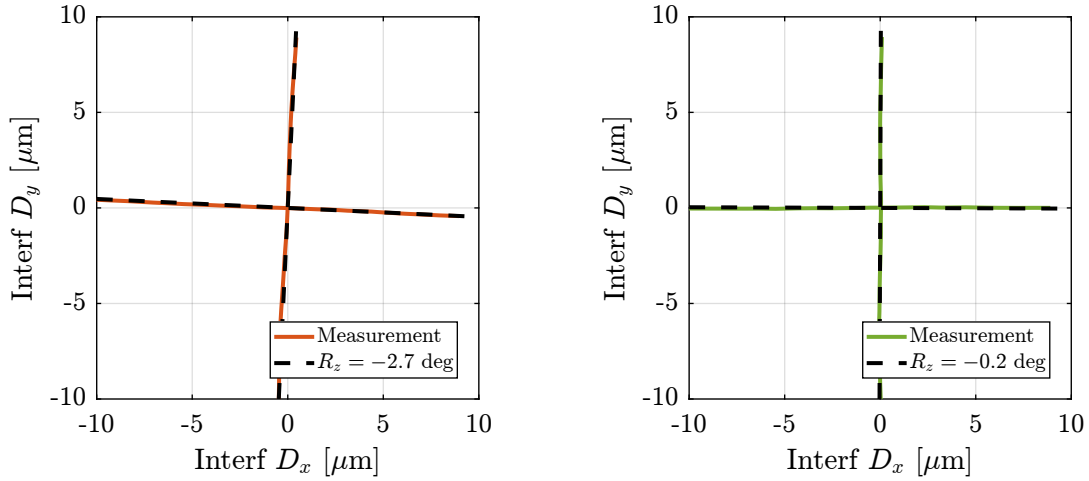

(a) Before alignment

(b) After alignment

Figure 2.2: Measurement of the Nano-Hexapod axes in the frame of the external metrology. Before alignment (a) and after alignment (b).

2.3 Open-Loop Identification after alignment

The plant dynamics is identified after the fine alignment and is compared with the model dynamics in Figure 2.3. Compared to the initial identification shown in Figure 2.1a, the obtained coupling has decreased and is close to the coupling obtained with the multi-body model.

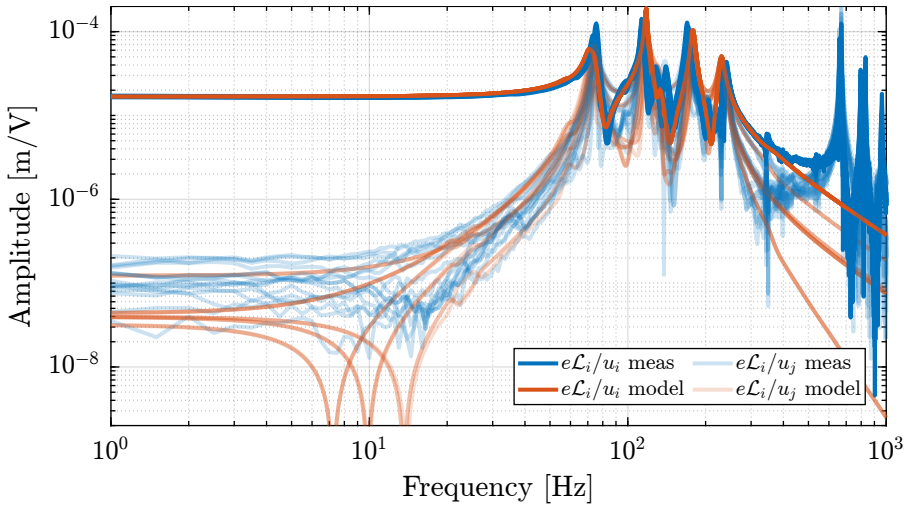

Figure 2.3: Decrease of the coupling with better Rz alignment

2.4 Effect of Payload Mass

The system dynamics was identified with four payload conditions that are shown in Figure 2.4. The obtained direct terms are compared with the model dynamics in Figure 2.5.

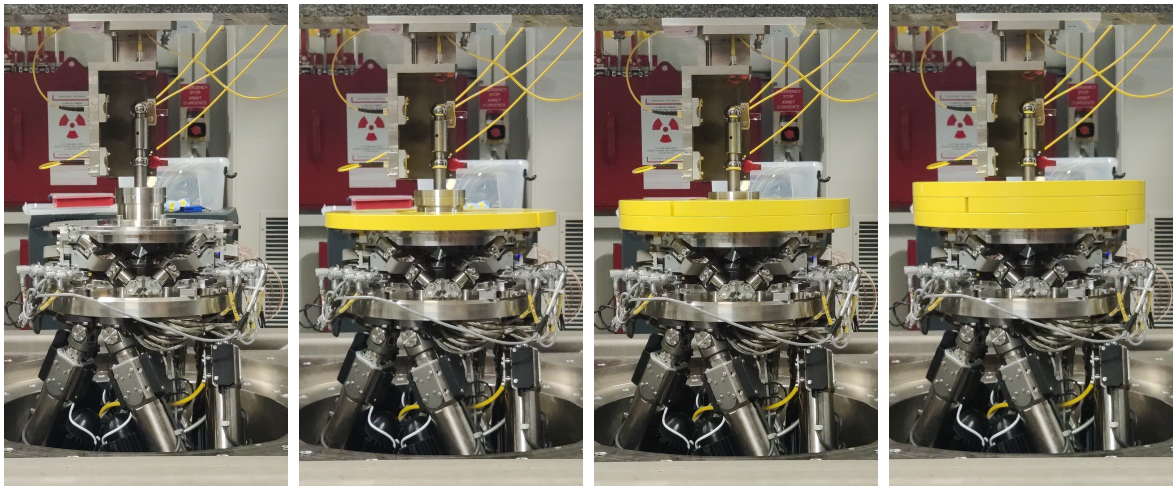

(a) $m = 0\,\text{kg}$ **(b)** $m = 13\,\text{kg}$ **(c)** $m = 26\,\text{kg}$ **(d)** $m = 39\,\text{kg}$

Figure 2.4: The four tested payload conditions. (a) without payload. (b) with 13 kg payload. (c) with 26 kg payload. (d) with 39 kg payload.

2.5 Effect of Rotation

The dynamics was then identified while the Spindle was rotating at constant velocity. Three identification experiments were performed: no spindle rotation, spindle rotation at $36\,\text{deg}/s$ and at $180\,\text{deg}/s$.

The comparison of the obtained dynamics from command signal u to estimated strut error $e\mathcal{L}$ is done in Figure 2.6. Both direct terms (Figure 2.6a) and coupling terms (Figure 2.6b) are unaffected by the rotation. The same can be observed for the dynamics from the command signal to the encoders and to the force sensors. This confirms that the rotation has no significant effect on the plant dynamics. This also indicates that the metrology kinematics is correct and is working in real time.

2.6 Conclusion

- Good match between the model and experiment

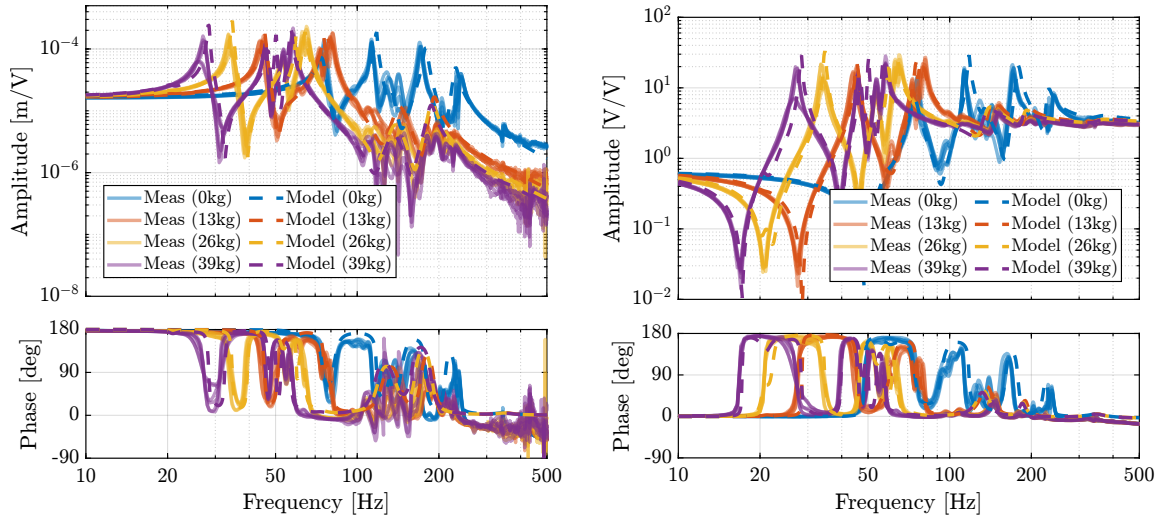

(a) from u to d_e **(b)** from u to V_s

Figure 2.5: Comparison of the diagonal elements (i.e. "direct" terms) of the measured FRF matrix and the dynamics identified from the Simscape model. Both for the dynamics from u to $e\mathcal{L}$ (a) and from u to V_s (b)

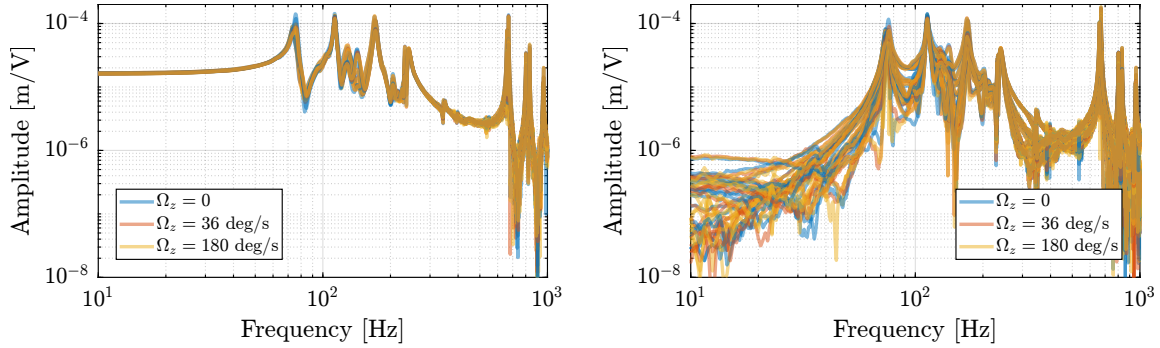

(a) Direct terms **(b)** Coupling terms

Figure 2.6: Effect of the spindle rotation on the plant dynamics from u to $e\mathcal{L}$. Three rotational velocities are tested ($0\,\text{deg}/s$, $36\,\text{deg}/s$ and $180\,\text{deg}/s$). Both direct terms (a) and coupling terms (b) are displayed.

Bibliography

[1] J. Watchi, S. Cooper, B. Ding, C. M. Mow-Lowry, and C. Collette, "A review of compact interferometers," *CoRR*, 2018. eprint: 1808.04175 (cit. on p. 9).